Inverse Poincaré Halfmaps

Claus Kahlert
Institute for Physical and Theoretical Chemistry, University of Tübingen

Z. Naturforsch. **42 a,** 143–152 (1987); received October 3, 1986

A family of critical curves that lie in the range of a class of Poincaré halfmaps induced by a saddle focus in three-space is investigated analytically. It comprises all "far final points" of the images of invariant curves that are subject to a separating mechanism. The number of branches occurring on a specific critical curve is directly related to the type of separating mechanism present in the halfmap. Moreover, universal properties of the saddle-focus dynamics are demonstrated for the first time.

1. Introduction

This is the third paper of a series investigating the properties of Poincaré halfmaps induced by the flow of a saddle-focus in three space. In the first two parts [1, 2] we treated structures responsible for the appearance of chaotic solutions. (In [3] a proof for a family of homoclinic trajectories in the present class of systems is given, so that the theorem that assures the existence of chaos in the neighborhood of a homoclinic orbit described in [4, 5] could be applied. See also [6] for a numerical example of a chaotic solution in the present piecewise-linear system.) Unlike the previous papers, in which the *domains* of the halfmaps were considered, in the following the emphasize will be on the *ranges* of these maps.

As mentioned in [2], the family of invariant curves of a halfmap is subdivided into those members that are subject to a separating mechanism and those that are not. For the latter type the halfmap acts more or less like a "reflection" along the line W (that separates the domain, S^-, and the range, S^+) [1]. Since this type of behavior does not entail any interesting dynamical consequences, it can be omitted here.

In the other, interesting case, the invariant curves are intersected by a branch cut, the critical spiral γ [2]. Adjacent points on both sides of this curve are separated, that is, are mapped elsewhere far apart from each other (see specifically Figs. 8–10 of [1] for the action of the halfmap $\bar{P}$ on an Ω-curve, a simple, and a complicated isola, respectively). While the image of a point from the critical spiral is located on the line segment W_s (see [2]), the exit point of the trajectory starting there is from S^+. If the overall system fulfills the existence and uniqueness criteria of [7], a point of contact of a trajectory with S is an exit and at the same time a re-entry point (whereby the second halfmap acts as the identity).

Specifically, the points s of the critical spiral fulfill the functional equation

$$\lim_{x \nearrow s} \bar{p}_0 \; \tilde{p}_0 \; \bar{p}(x) = \lim_{x \searrow s} \bar{P}(x) \,, \tag{1}$$

where $x \nearrow s$ ($x \searrow s$) means a counterclockwise (clockwise) approach towards s along an invariant curve. Obviously, the points $\lim_{x \searrow s} \bar{P}(x)$ yield a *new critical curve*, φ, for the *inverse* dynamics.

If one constructs φ explicitly, for *all* values of the canonical parameters, one finds both physically meaningful together with meaningless segments. The relevant portions must then be found applying a specific selection rule. It will turn out that the number of branches that contribute to φ equals unity plus the number of self-intersection points characteristic for the corresponding critical spiral. Moreover, the selection rule yields a charting of the canonical parameter space that is equivalent to the one presented in [2]. At the same time it allows to demonstrate the existence of *universal properties* of the saddle-focus dynamics.

A main technical result will be the location of "far final points" (that is, the exit points of trajectories starting at "first cutting open points" [2]). This means that the images of all invariant curves that intersect the critical spiral are known completely.

Reprint requests to Dr. C. Kahlert, Institut für Physikalische und Theoretische Chemie der Universität Tübingen, Auf der Morgenstelle 8, D-7400 Tübingen, F.R.G.

0340-4811 / 87 / 0200-0143 $ 01.30/0. – Please order a reprint rather than making your own copy.

2. The Curve $\tilde{\varphi}$

In order to utilize the techniques developed previously, we treat the range of the halfmap, that is to be considered here, as the domain of its inverse. Since the flow that induces $\bar{P}$ [1] is unique, its temporal inverse exists and obeys the following canonical equation of motion:

$$\frac{dx}{dt} = \varrho x \quad \text{and} \quad \frac{dy}{dt} = -(1 + i\omega) y \tag{2}$$

with $x \in \mathbb{R}$, $y \in \mathbb{C}$, $\varrho > 1$, and $\omega > 0$. This dynamics is assumed to be active inside the region $\bar{T}$ [1] and induces a one-to-one map, $\bar{P}^{-1}$, from S^+ into S^-. Since (2) is the time-inverse of the former Eq. (32) in [1], all geometric structures (specifically all invariant curves Γ) remain the same as before, treated explicitly in [1]. Although the dynamics to be considered here is given by (2), whenever we talk about "trajectories" we shall implicitly adopt the opposite time direction – in order to obtain an interpretation that is consistent with the previous papers.

Let us now formulate the halfmap induced by the flow of (2). The function u (controlling the switching of dynamics) in the present case reads

$$u(t) := x\, e^{\varrho t} + 2\, e^{-t} (\eta(x) \cos \omega t + \xi \sin \omega t)\,, \tag{3}$$

cf. [1]. (For the definitions of $\eta(x)$ and ξ, see Eqs. (22) and (41) of [1].) The implicit equation which describes the halfmap $\bar{P}^{-1}$ in terms of the mapping time τ becomes

$$u(0) = u(\tau) = x_0\,. \tag{3a}$$

The formalism of critical curves (developed in [8, 9]) now yields for the "numerator and denominator functions" z and n:

$$z(\tau) = \omega - e^{\tau} (\omega \cos \omega\tau - \sin \omega\tau) \tag{4a}$$

and

$$n(\tau) = \omega - e^{(\varrho+1)\tau} (\omega \cos \omega\tau - (\varrho + 1) \sin \omega\tau)\,. \tag{4b}$$

Thus the τ-representation of the curve, containing the intersection points of touching trajectories with S, may be written as

$$\tilde{\varphi}(\tau) = (x_\tau, \xi_\tau(x_\tau))^{\mathrm{T}}\,, \tag{5}$$

whereby

$$x_\tau = x_0 \frac{z(\tau)}{n(\tau)} \tag{6a}$$

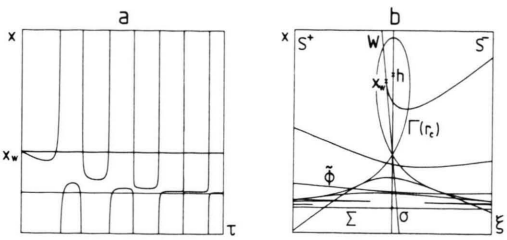

Fig. 1. (a) Plot of the function x_τ for $x_0 = 1$, $\varrho = 1.5$, and $\omega = 10$. Axes: $\tau = 0 \ldots 8\pi/\omega$, $x = -x_w \ldots 4x_w$. (b) The curve $\tilde{\varphi}$ corresponding to x_τ of part (a) together with the Cartesian leaf. Note that not all branches shown here contribute to the critical curve φ. Axes: $x = -0.2\,x_w \ldots 1.4\,x_w$, $\xi = -1 \ldots 1$.

and

$$\xi_\tau(x_\tau) = \frac{-e^{(\varrho+1)\tau} + \cos \omega\tau}{2 \sin \omega\tau} x_\tau + \frac{e^{\tau} - \cos \omega\tau}{2 \sin \omega\tau} x_0\,, \tag{6b}$$

(cf. Eqs. (15), (18), and (19) in [2]). Compared to the analogous expression for z and n in [2] (see also [9] for another one), "just a few signs" are changed. These modifications, nevertheless, result in a completely different behavior of x_τ and of all structures derived from this central quantity. A concrete visual example of x_τ and $\tilde{\varphi}$ is presented in Figure 1. The latter curve shown is called $\tilde{\varphi}$ since the critical curve φ, that we are looking for eventually has to be extracted from this object by applying specific selection rules (see below).

For $\tau \to 0$ both z and n vanish to second order, so that

$$\lim_{\tau \to 0} x_\tau = x_0 \frac{\omega^2 + 1}{(\varrho + 1)^2 + \omega^2} = x_w \tag{7a}$$

and

$$\lim_{\tau \to 0} \xi_\tau(x_\tau) = \frac{\varrho\, x_0}{2\omega} \frac{\varrho + 1 - \omega^2}{(\varrho + 1)^2 + \omega^2} = \xi_w(x_w)\,. \tag{7b}$$

Hence $\tilde{\varphi}$ starts, like the critical spiral, in the final point of the separating portion of the straight line W [2].

In contrast to the situation valid for the critical spiral, n vanishes at positive values of τ too. Since in general z possesses no zeros at these points, x_τ diverges there. The pertinent poles of x_τ are not accessible analytically. However, in the limit $\tau \to \infty$, the ω-term in (4b) may be neglected com-

pared to the exponential. Therefore the zeros τ_k^∞ of n converge towards

$$\tau_k^{\infty\,\infty} = \frac{1}{\omega}\left[\arctan\frac{\omega}{\varrho+1} + k\,\pi\right]. \tag{8a}$$

On the other hand, the zeros τ_k^0 of the numerator function z tend towards the values

$$\tau_k^{0\,\infty} = \frac{1}{\omega}\left[\arctan\omega + k\,\pi\right]. \tag{8b}$$

Hence the limiting structure of the poles and the zeros of x_τ is known explicitly. This will be a great help in analyzing φ itself.

3. The Critical Curve φ

In order to obtain φ, we have to select those exit points of touching trajectories that contribute regularly to the halfmap [2]. Two selection rules can be read off immediately from Fig. 1:

(S1) Only nonnegative values of x_τ contribute to φ. This is obvious because adjacent trajectories with initial x-coordinates less than zero cannot be separated [1].

(S2) All points $\tilde{\varphi}(\tau)$ from S^- must be eliminated. This selection rule stems from the fact that by definition all *exit* points of $\bar{T}$ are from S^+. The excluded points are *entry* points of $\bar{T}$ and thus belong to trajectories that spent some time inside $\tilde{T}$ under the dynamics of $\bar{T}$, i.e., they come from nonmanifest shadow solutions [7].

A third and final selection rule can be obtained by looking at the image of $\tilde{\varphi}$ under $\bar{P}^{-1}$. This image is by construction located on W, hence it is sufficient to investigate its x-component

$$x_s(\tau) := x_\tau e^{\varrho\tau} \tag{9}$$

alone. We therefore have:

(S3) Only the first appearance of a value $x_s(\tau)$ from $[0, x_w)$ is to be considered as physically meaningful. Only in this case do trajectories, that start on W_s, cross S for the *first* time after the mapping time τ has elapsed.

The criterion (S3) implies the previous two:

ad(S1) No point $\tilde{\varphi}(\tau)$ with $x_\tau < 0$ is mapped by $\bar{P}^{-1}$ into W_s, because $x_s(\tau)$ always possesses the same sign as x_τ. Hence the first criterion is a consequence of the third one.

ad(S2) To see how the second one can also be derived, suppose a touching trajectory that starts on W_s and crosses S^- in s after time τ. Then, in order to enter $\tilde{T}$, the trajectory also crosses S^+, prior to τ, after time τ' in the point s'. Hence s' too belongs to $\tilde{\varphi}$ and may be written as $\tilde{\varphi}(\tau - \tau')$. Since $\tau' > 0$, s does not contribute to φ. (Note that nothing is said about whether s' belongs to φ or not.)

The criterion (S3) is also complete – in the sense that it selects a minimal set of points and thus yields a one-to-one map onto W_s. Any further point excluded from $\tilde{\varphi}$ would result in a hole inside of $[0, x_w)$, meaning that a regularly touching trajectory would not be represented. We therefore have obtained the exact criterion to be applied to $\tilde{\varphi}$ in order to select φ from it.

Analogously to the situation found for the critical spiral, the present selection rule cuts out certain τ-intervals (mapping times). These intervals cannot be determined explicitly. They can, however, be gained easily with the aid of a computer, as will be shown below.

In order to obtain φ via x_s, the x-component of its image, we also need the derivative of the latter function. So we define:

$$D_3(\tau) := \frac{\mathrm{d}}{\mathrm{d}\tau} x_s(\tau) = \frac{x_0\, e^{\varrho\tau}}{n^2(\tau)}\, d_3(\tau) \tag{10}$$

with

$$\begin{aligned} d_3(\tau) := {} & \varrho\omega + e^\tau\{(\omega^2+\varrho+1)\sin\omega\tau - \varrho\omega\cos\omega\tau\} \\ & - e^{(\varrho+1)\tau}\{(\omega^2+\varrho+1)\sin\omega\tau + \varrho\omega\cos\omega\tau\} \\ & + e^{(\varrho+2)}\varrho\omega\,. \end{aligned} \tag{10a}$$

It is mainly from this function that the properties of the selection rule (S3) will be extracted.

If we compare D_3 with D_1 as given in [2] (Eq. (30)), the expression in square brackets there turns out to differ from d_3 here only by a factor $e^{(\varrho+2)\tau}$, so both functions possess the same number of zeros. Surprisingly, they also occur at the same values of τ – this shows the symmetry between the two critical curves γ and φ. As far as the behavior of the zeros is concerned, all the properties of D_1 carry over to D_3, thus we can make use of the results elaborated there. It hereby goes without saying that D_3 only has a zero if the denominator (note that the function n possesses a countable infinite number of zeros on the

positive τ-axis) does not vanish together with the numerator and so at least to the same order. This situation – when the numerator and the denominated of D_3 vanish simultaneously – will be discussed below. At the moment we assume these two functions to possess distinct zeros.

In order to investigate x_s, let us first look at its limiting behavior. From (7) we know that $\lim_{\tau \to 0} x_s(\tau) = x_w$ and for its derivative we find, after removing fourth order singularities:

$$\lim_{\tau \to 0} D_3(\tau) = \frac{\varrho}{3} x_w . \tag{11}$$

This yields a simple connection between the initial value of x_s and its initial slope; moreover, (11) shows that, for all possible values of the canonical parameters, x_s starts at the x-valued supremum of W_s with a *positive* slope. On the other hand, for $\tau \to \infty$ the behavior of d_3 is dominated by its final term, $\varrho\, \omega\, e^{(\varrho+2)\tau}$. In this limit D_3 converges towards $x_0\, \varrho\, \omega^2/(\omega \cos \omega\, \tau - (\varrho+1) \sin \omega\, \tau)^2$, which is strictly positive. It is because of this property that D_3 possesses at most a finite number of intervals in which it assumes negative values.

After having inspected the limits, let us now discuss the different bifurcations possible for x_s by following a (vertical) path in the (ϱ, ω)-subspace of canonical parameters (see [2], Fig. 6). For small values of the focal frequency (below the curve $\omega^2 = \varrho + 1$), D_3 has no zero (and thus is strictly positive) for all $\tau > 0$. Hence the first branch of x_s, from the interval $(0, \tau_1^\infty)$, does not contribute to φ; all its values are greater than x_w. The second branch, for $\tau_1^\infty < \tau < \tau_2^\infty$, covers the whole real axis including $[0, x_w)$; thus this branch is the only one that contains regular points. Looking at φ itself we find its domain to be the interval $[\tau_1^0, \tau_1^w) \subset (\tau_1^\infty, \tau_2^\infty)$, with $x_s(\tau_1^w) = x_w$. There the characteristic radius of φ increases strictly from zero. So the critical curve intersects all base lines, the Cartesian leaf, and a fraction of the Ω-curves – where it ends on the one possessing the radius r_w (cf. Eq. (13) of [2]).

For values of ω above $\sqrt{\varrho+1}$, but below the Ω_1-curve, D_3 still possesses no zero, hence again the second branch of x_s alone contributes to φ. In contrast to the situation described above, however, now x_w is greater than x_c and hence the characteristic radius of φ decreases for values of x_s inside (x_c, x_w) (see [2], Eqs. (26), (28) and Figure 4). In this case φ touches the Cartesian leaf (in s_c') and thereafter crosses base lines of radius $r_c > r_0 > r_w$ for a *second* time.

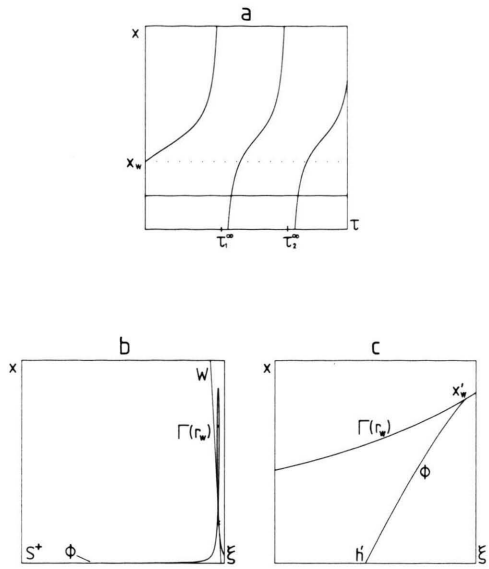

Fig. 2. This and the following three figures visualize the behavior of the functions x_s and φ for typical values of ϱ and ω, taken from the different regions of the canonical parameter space. Present parameters: $x_0 = 1$, $\varrho = 1.5$, $\omega = 1.1$. (a) For $\omega^2 < \varrho + 1$ the second branch of x_s (for $\tau = \tau_1^\infty$ to τ_2^∞) already covers the interval $[0, x_w)$. Axes: $\tau = 0 \ldots 3\pi/\omega$, $x = -x_w \ldots 5x_w$. – (b) The curve φ possesses one branch that starts on the line Σ ($x = 0$) and ends at the Ω-curve $\Gamma(r_w)$. Axes: $x = 0 \ldots 5x_w$, $\xi = -30 \ldots 1$. – (c) Blow-up of (b). Axes: $x = 0 \ldots 0.003\, x_w$, $\xi = -30 \ldots -20$.

If we increase ω beyond Ω_1, a pair of zeros appears in D_3. While the first one yields a maximum of x_s (with x-value less than x_w) on the second branch, the second zero of D_3 results in a minimum (having a value greater than x_w) on the third branch.

Utilizing this information, we can now apply the selection rule (S3) formulated above: The first branch of x_s again yields no contribution. From the second branch it is the interval $[\tau_1^0, \tau_1^e]$, ranging from the first zero to the first extremum (maximum), that is selected. The rest of this branch is "shaded off" (suppressed) since there, for all values of τ greater than τ_1^e, the $x_s(\tau)$ are second appearances. The third branch of x_s is completely excluded (all its values are greater than x_w). Finally, from the fourth branch – which again covers all real values – we pick the pre-image of $[0, x_w) \setminus [0, x_s(\tau_1^e)]$, that is (τ_1^f, τ_1^w). Thus,

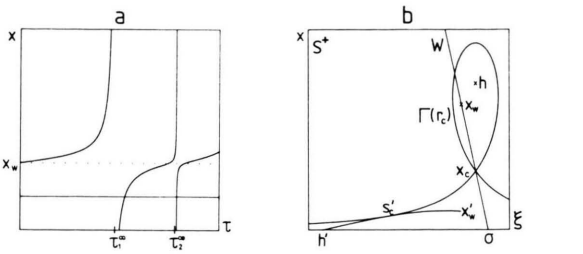

Fig. 3. For $\omega^2 > \varrho + 1$ all critical curves are found inside the Cartesian leaf. Parameters: $x_0 = 1$, $\varrho = 1.5$, $\omega = 5.5$. – (a) The function x_s behaves qualitatively similar to the situation found in Figure 2 (a). Axes: $\tau = 0 \ldots 3\pi/\omega$, $x = -x_w \ldots 5x_w$. – (b) The critical curve φ touches the Cartesian leaf in s'_c and then returns to the interior of the leaf. The latter section reflects type II separation. Axes: $x = 0 \ldots 1.6\, x_w$, $\xi = -1.25 \ldots 0.25$.

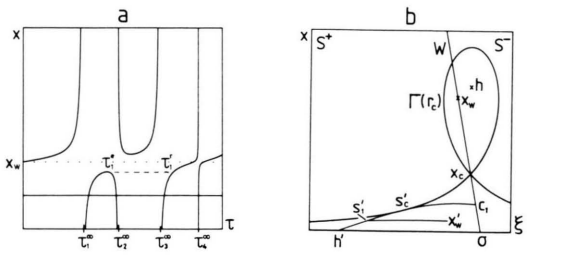

Fig. 4. Beyond the curve Ω_1, new phenomena appear. Parameters: $x_0 = 1$, $\varrho = 1.5$, $\omega = 8$. – (a) A maximum on the second and a corresponding minimum on the third branch of x_s appear. Note that only the first appearance of a value from the interval $[0, x_w)$ contributes to φ. Axes: $\tau = 0 \ldots 5\pi/\omega$, $x = -x_w \ldots 5x_w$. – (b) Since the domain of φ is disconnected, the critical curve itself possesses two branches. Note that s'_1 is the image of c_1. Axes: $x = 0 \ldots 1.5\, x_w$, $\xi = -1 \ldots 0.25$.

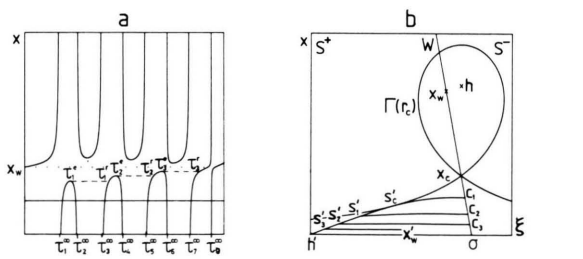

Fig. 5. Example for a parameter set beyond the curve Ω_3. Parameters: $x_0 = 1$, $\varrho = 1.5$, $\omega = 12$. – (a) x_s possesses three local maxima (at τ_1^e, τ_2^e, and τ_3^e) with increasing values and three corresponding local minima with decreasing values. Axes: $\tau = 0 \ldots 9\pi/\omega$, $x = -x_w \ldots 5x_w$. – (b) For every pair of extrema of x_s an additional new branch of φ appears, hence it possesses four branches. Axes: $x = 0 \ldots 1.4\, x_w$, $\xi = -0.6 \ldots 0.2$.

φ is defined on two disjoint intervals. This is reflected in two branches of the critical curve existing in this case. Note that $\tau_1^r\,(> \tau_1^e)$ is defined by $x_s(\tau_1^r) = x_s(\tau_1^e)$, so that the final point c_1 of the first branch of φ is located on the same base line as the starting point s'_1 of the second branch (s'_1 is the image of c_1 under $\bar{P}$). The onset of a second branch of φ was first observed numerically in [10] and called a "hook" there.

If we increase the value of ω even further and cross the curve Ω_2, the second branch of φ approaches W_s and a third one arises, starting in s'_2 (the image of the final point c_2 of the second branch). In this case D_3 possesses two pairs of zeros. In general a new branch of φ always comes into existence together with a pair of zeros in D_3 – that is, whenever we cross a curve Ω_k in the canonical parameter space. This is a consequence of the fact than x_w while subsequent local *maxima* of x_s form an increasing series of values less than x_w. Therefore close to their maxima the branches are not shaded off so that each one of these, together with the first branch after the final minimum, corresponds to a separate branch of φ. Hence: *The number of branches found in φ is equal to unity plus the number of curves Ω_k crossed.*

Now we are in the position to present the promised modified selection rule:

(S3′) A point $x_s(\tau)$ contributes to φ if it is both from $[0, x_w)$ and greater than all the previously accepted ones. This criterion is an immediate consequence of the fact that x_s, restricted to the domain of φ, is strictly increasing. One immediately sees why (S3′) is an adequate formulation for a computer. We need not have to fill an interval with real numbers, which is impossible for a finite state machine; nor do we have to cover it with a great number of tiny intervals, which would be memory exhausting; rather, scanning a scalar function, we only have to keep track numerically of the actual maximum value that appears inside the interval of interest.

4. The Curves Ω_k Revisited

A remarkable property follows from (10) above. The curves Ω_k in parameter space are characterized by degenerate zeros of D_1 [2] or, equivalently, D_3.

A sufficient condition for this situation to appear is a simultaneous zero of z and n. Hence the Ω_k may be obtained by looking for parameters where τ_{2k}^0 and τ_{2k}^∞ coincide (at τ_k^c). This can be done much faster than to solve the more complicated Eqs. (34) and (36) of [2] simultaneously. In consequence the charting of the canonical parameter space, that was obtained previously from the properties of the critical spiral [2], is now reproduced by the behavior of φ (compare Fig. 6 here to Fig. 6 of [2]).

Along the Ω_k we find, without knowing the τ_k^c themselves,

$$x_s(\tau_k^c) = x_0 \exp[\varrho\,\tau_k^c] \lim_{\tau \to \tau_k^c} \frac{z(\tau)}{n(\tau)} = x_w . \qquad (12)$$

This makes sense since for parameters from Ω_k the critical curve φ ends on W_s at the final point of its k-th branch – and the end point of φ is the "image" of x_w. For the derivative of x_s we find in the present case

$$D_s(\tau_k^c) = \frac{\varrho}{2} x_w , \qquad (13)$$

which differs from the value $(\varrho/3)\, x_w$ of (11). This is due to the fact that at $\tau_0^c (= 0)$, the denominator function n vanishes to second order whereas for all $k > 0$ the zeros of n are simple.

To visualize the consequences of the bifurcations that appear along the curves Ω_k, let us look at the implicit equations

$$z(\tau_{2k}^0; \varrho, \omega) = 0 \qquad (14a)$$

and

$$n(\tau_{2k}^\infty; \varrho, \omega) = 0 , \qquad (14b)$$

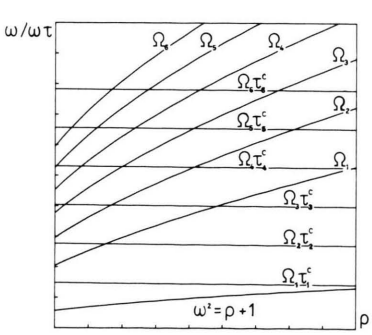

Fig. 6. The first six curves Ω_k calculated as simultaneous zeros of z and n. Further Ω_k up to arbitrarily large k can be calculated in the same manner. Note that along these curves the phase $\Omega_k \tau_k^c$ remains approximately constant. Axes: $\varrho = 1 \ldots 10$, $\omega = 0 \ldots 25$ / $\omega\tau = 0 \ldots 50$.

and let us choose ϱ as the pertinent bifurcation parameter. From the Implicit Function Theorem, the "shift" of the zeros of z and n due to a variation of ϱ is obtained as:

$$\frac{d\tau_{2k}^0}{d\varrho} = 0 \qquad (15a)$$

and

$$\frac{d\tau_{2k}^\infty}{d\varrho} = \frac{1}{\omega^2 + (\varrho+1)^2} \cdot \left[\frac{\omega\,\tau_{2k}^\infty}{\exp[(\varrho+1)\,\tau_{2k}^\infty] \sin \omega\,\tau_{2k}^\infty} - 1 \right] . \qquad (15b)$$

The latter expression can be evaluated at $\tau_{2k}^\infty = \tau_k^c$, using

$$\exp[(\varrho+1)\,\tau_k^c] \sin \Omega_k \tau_k^c = \frac{\Omega_k}{\varrho} (\exp[\varrho\,\tau_k^c] - 1) \qquad (16)$$

which follows from (14). This yields, on the curve Ω_k (i. e., for $\omega = \Omega_k(\varrho)$)

$$\frac{d\tau_{2k}^\infty}{d\varrho} = \frac{-1}{\Omega_k^2(\varrho) + (\varrho+1)^2} \sum_{j=2}^{\infty} \frac{(\varrho\,\tau_k^c)^j}{j!} < 0 . \qquad (17)$$

We can therefore understand how the values of τ_{2k}^0 and τ_{2k}^∞ reverse their mutual ordering when a point in parameter space crosses Ω_k. Moreover it turns out that *all* curves Ω_k are characterized by the law $\tau_{2k}^0 = \tau_{2k}^\infty$ – a local maximum of x_s on one branch and a minimum on the next one can only appear if the zeros reverse their "natural" ordering that is given by the limiting behavior $\tau_k^\infty < \tau_k^0$ described by (8).

As a final result a very interesting property of the curves Ω_k becomes apparent from Figure 6: *The phases $\Omega_k \tau_k^c$ remain virtually constant for all values of ϱ, with subsequent curves appearing almost equidistant.* This behavior is independent of the particular saddle-focus investigated. It therefore constitutes a *universal feature* of any saddle-focus type dynamics.

In order to obtain these universal properties explicitly, let us again employ the Implicit Function Theorem. Solving (14) numerically, we find that the difference between subsequent values of $\Omega_k \tau_k^c$ converges towards 2π from above. (In the limit $\varrho \to \infty$, the simultaneous zeros of z and n are

located at integer multiples of 2π.) For the derivative of $\Omega_k \tau_k^c$ we find:

$$\frac{\mathrm{d}}{\mathrm{d}\varrho}[\Omega_k(\varrho)\,\tau_k^c(\varrho)]$$

$$= \frac{\partial n(\tau_k^c;\varrho,\Omega_k)}{\partial \varrho}\frac{1}{J}(\Omega_k\tau_k^c - \exp[\tau_k^c]\sin\Omega_k\tau_k^c)\,, \quad (18)$$

where

$$J := \det\frac{\partial(z,n)}{\partial(\tau_k^c,\Omega_k)}\,, \quad (18a)$$

is the determinant of the Jacobian matrix. We then may apply

$$\exp[\tau_k^c]\sin\Omega_k\tau_k^c = \frac{\Omega_k}{\varrho}(1-\exp[-\varrho\tau_k^c])\,, \quad (19)$$

which is analogous to (16), to obtain

$$\frac{\mathrm{d}}{\mathrm{d}\varrho}[\Omega_k(\varrho)\,\tau_k^c(\varrho)] = \frac{\partial n(\tau_k^c;\varrho,\Omega_k)}{\partial\varrho} \cdot \frac{1}{J}\frac{\Omega_k}{\varrho}\sum_{j=2}^{\infty}\frac{(-\varrho\tau_k^c)^j}{j!}\,. \quad (20)$$

Taking into consideration that

$$\frac{\partial n(\tau_k^c;\varrho,\Omega_k)}{\partial\varrho} = \frac{\Omega_k}{\varrho}(\exp[\varrho\tau_k^c]-1) - \Omega_k\tau_k^c = \frac{\Omega_k}{\varrho}\sum_{j=2}^{\infty}\frac{(\varrho\tau_k^c)^j}{j!}\,, \quad (21)$$

we see that the power series expansion of the numerator of (18) starts with a second-order term, while J itself vanishes linearly as ϱ approaches zero. Hence for small values of ϱ the derivative of $\Omega_k\tau_k^c$ tends towards zero. For the other limit, $\varrho\to\infty$, the numerator of (20) behaves like Ω_k^2/ϱ^2. In this case J converges towards

$$J_s = \exp[\varrho\tau_k^c]\frac{\Omega_k\tau_k^c}{\varrho} \cdot \{\varrho\Omega_k - (\varrho^2+\Omega_k^2)(\Omega_k\tau_k^c - 2k\pi)\} \quad (22)$$

and thus the derivative in question vanishes there too.

The simple behavior of $\Omega_k\tau_k^c$ obviously reflects the similarity of freshly created doubly touching trajectories. The difference between them is dominated by an extra turn around the real eigenvector of the saddle-focus.

5. The Complete Halfmap

Now that we have obtained a complete picture of φ, let us have a look at how the segments of the other critical curve, the spiral γ, are mapped onto it. Instead of treating the different cutting open

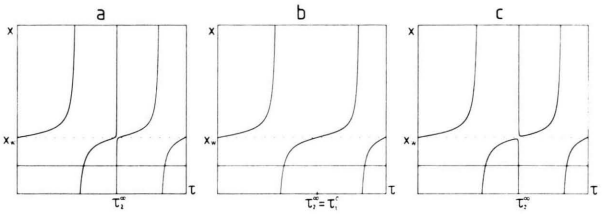

Fig. 7. For values of the parameters close to Ω_1, the (complex) zeros of x_s and D_3 are also close to one another. Axes for all parts: $\tau = 0\ldots 4\pi/\omega$, $x = -x_w\ldots 5x_w$. – (a) Just below the bifurcation point on Ω_1 the "knees" of the second and the third branch of x_s, respectively, come close to the pole located at τ_2^∞. Parameters: $x = 1$, $\varrho = 1.5$, $\omega = 5.7$. – (b) Exactly at a point of Ω_1, the zeros in the numerators cancel those of the denominators in x_s as well as in D_3. Hence no singularity appears at τ_2^∞. Parameters: $x_0 = 1$, $\varrho = 1.5$, $\omega = 5.74241506581$. – (c) Slightly above Ω_1, we again find a pole of x_s at τ_2^∞ together with a pair of local extrema closely adjacent to this point from the left and the right, respectively. Parameters: $x_0 = 1$, $\varrho = 1.5$, $\omega = 5.8$.

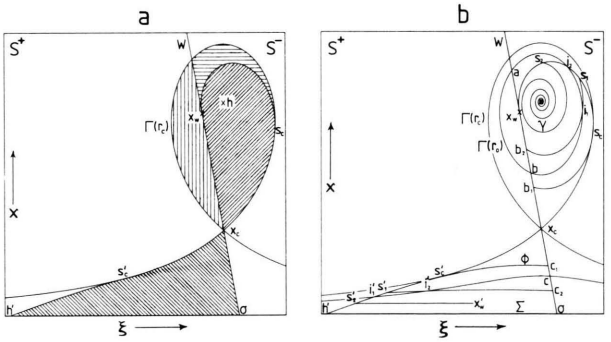

Fig. 8. For high frequencies of the saddle focus (after having crossed Ω_2) both critical curves γ and φ possess different branches that start and end at entry points, points of contact, or exit points, respectively, of doubly touching trajectories. Parameters: $x_0 = 1$, $\varrho = 1.5$, $\omega = 10$. Axes: $x = 0\ldots 1.4\,x_w$, $\xi = -0.7\ldots 0.2$. – (a) The images of the different regions inside the Cartesian leaf $\Gamma(r_c)$, being mapped onto isolae or base lines, respectively, are known exactly. – (b) The segments $\widehat{hs_1}$, $\widehat{b_1 s_2}$, $\widehat{b_2 s_c}$, $\widehat{s_c s_2}$, $\widehat{s_2 s_1}$, and $\widehat{s_1' x_w}$ of γ are mapped by $\bar{p}_0\bar{p}_0\bar{p}$ onto $\widehat{h's_1'}$, $\widehat{s_1' s_2'}$, $\widehat{s_2' s_c'}$, $\widehat{s_c' c_1}$, $\widehat{s_1' c_2}$, and $\widehat{s_2' x_w'}$ of φ. This shows how the boundary $x_w s_c$ of part (a) is eventually mapped onto the "gluing together" segments inside the region of base line. Specifically the isola $\Gamma(r_0)$ $(r_0 = 0.8\,r_c)$ shows how a separation and gluing-together appears: $\widehat{b i_1}$ is mapped onto $\widehat{i_2' c}$, $\widehat{i_1 i_2}$ goes to $\widehat{i_1' i_2'}$, and $\widehat{i_2 a}$ is mapped onto $\widehat{b a}$.

mechanisms separately, a typical type III situation (corresponding to the assumption that we have crosses the first k curves Ω_i in parameter space) will be discussed. Its properties cover those of the two others. In the present Section the critical spiral is to be treated in *reversed* τ-direction: that is, we start at the center represented by large mapping times, and move towards the peripheral turns which show small values of τ.

The innermost turns of γ, up to the point s_k (see Fig. 8 b), are mapped onto the interval $(0, c_k]$ of W_s. This latter portion is mapped again, by $\bar{P}$, onto the arc $\widehat{h' s'_k}$ of φ. On reaching s_k, the critical spiral becomes disconnected (a τ-interval is cut out of its domain [2]) and it continues in b_k (on the same isola). The arc $\widehat{b_k s_{k-1}}$, extending from the re-start point to the next point of self-intersection, is then mapped onto $(c_k, c_{k-1}]$ and further onto $\widehat{s'_k s'_{k-1}}$; and so on. Eventually as the spiral re-starts in b_1, the arc from there to s_c, the point of contact with the Cartesian leaf, is mapped onto $(c_1, x_c]$ and from there onto $\widehat{s'_1 s'_c}$.

Up until now, all points of the critical spiral were "primary cutting open points" [2], with adjacent points of the intersected isola to the left and the right being mapped to opposite ends of the image of this invariant curve, inside the base line region of S^+. It is this behavior that originally motivated the present paper: The "triangle" $x_c x_w s_c$ is mapped onto the region bounded by the lines Σ (defined by $x = 0$; the image of the homoclinoid point h) and W, moreover by the arc $\widehat{x_c s'_c}$ of $\Gamma(r_c)$ and the section $\widehat{h' s'_c}$ of φ. Thus *the image of the whole region inside of which a separation occurs is determined analytically to be the "quadrangle"* $\sigma x_c s'_c h'$ (see Figure 8).

The points of the critical spiral to be discussed next are "secondary cutting open points" [2]. They separate those parts of a complicated isola which are mapped onto the segment of the same isola inside S^+ and those that are mapped onto the corresponding base line, respectively. The distinction between primary and secondary cutting open points is immediately reflected in φ: The images of the first sort are from the boundary discussed while those of the second type are from the interior of $\sigma x_c s'_c h'$. At the latter points, the images of the arcs $\widehat{b i}$, and $\widehat{i_1 i_2}$ of the isola $\Gamma(r_0)$ (see Fig. 8 b) are glued together with a reversed mutual orientation.

Although the domain of the critical spiral was disconnected, the image of γ up to s_c is simply the interval $(0, x_c]$. The corresponding curve φ also possesses a simply connected domain up to this point. Continuing from here on, however, γ behaves smoothly while φ is subject to a selection rule that cuts certain τ-intervals out of its domain.

The arc $\widehat{s_c s_1}$ of γ is mapped to $(x_c, b_1]$ and from there to $\widehat{s'_c c_1}$; this completes the first branch of φ. The subsequent arcs of γ in between the revisited self-intersection points s_i and s_{i+1} are mapped onto the intervals $(b_i, b_{i+1}]$ and from there onto separate branches $\widehat{s'_i c_{i+1}}$ $(i = 1 \ldots k-1)$ of φ. Finally the section $\widehat{s_k x_w}$ is mapped onto (b_k, x_w) and further onto the last branch of φ being $\widehat{s'_k x'_w}$. This completes our visualizing of the halfmap.

The above results show that the two critical curves, γ and φ, appear somewhat "conjugate". The innermost turns of the critical spiral (its "end") is mapped to the "beginning" of φ and vice versa. (Still, since for φ neither the zero mapping time is the infimum nor infinity is the supremum of its domain, as this was the case for γ, we cannot go so far as to expect a simple "sum rule" or a related law to hold true.) Another point where the conjugacy makes itself felt is the occurrence of a type III separation: At the self-intersection points s_i of the critical spiral a type I branch is "pinned" onto the type II curve, while in the points s'_i of φ, type II branches start off from the type I curve. Note that s_i and s'_i appear in γ (and φ, respectively) exactly at the same values of τ – this is a highly symmetric situation.

6. Discussion

This paper concludes the treatment of separating mechanisms in Poincaré halfmaps induced by a saddle-focus in three space. These mechanisms were shown to be responsible for the appearance of chaotic solutions in the overall dynamical system – provided an appropriate second halfmap is present [11].

The formalism of halfmaps both is consistent and yields a complete description of the dynamical behavior. Let us therefore finally visualize it in terms of the temporal evolution of the dynamical system itself. The crucial point is the behavior of

touching trajectories. For type I separations, such an orbit starts in a point of γ, touches S inside W_s, and returns from there to $\bar{T}$ in order to eventually exit this region in a point of φ. Thus trajectories adjacent at "both sides" of the latter orbit exit $\bar{T}$ either close to W or close to φ, in between these two curves.

For the second type of separation we find two kinds of touching trajectories, those behaving like the ones discussed above (they touch S below x_c), and those touching S inside of (x_c, x_w) on W_s. The latter points of contact are located on the intersection of a complicated isola with W_s. In this case adjacent trajectories either cross S^+ close to the point of contact, b_k, in the interval (x_c, x_w) of W_s, and possess a second one, c_k, in $(0, x_c)$. To better line. These exit points are located in the neighborhood of exit points of trajectories that start inside S^-, close to the segment (x_c, x_w) of W_s. Thus the exit point of a trajectory, entering $\bar{T}$ in a secondary cutting open point, is a gluing-together point at which the images of points that lie far from each other meet.

The third type of separation in Poincaré halfmaps, which is the most interesting one, is connected to a special type of touching orbits – *doubly* touching trajectories. They start in a self-intersection point s_k of the critical spiral, have their first point of contact, b_k, in the interval (x_c, x_w) of W_s, and possess a second one, c_k, in $(0, x_c)$. To better understand why type III separation is a combination of type I and type II, it is helpful to remark that in the neighborhood of a doubly touching trajectory, simply touching orbits appear that possess their points of contact either in the second or in the first of the above mentioned two intervals. Corresponding to the three "arms" of the critical spiral that meet at a point s_k, we find three major types of behavior:

(a) A representative of the first kind comes close to b_k but remains inside $\bar{T}$ in order to touch S a little below c_k. This trajectory eventually exits on the first branch of φ, hence it shows type I behavior. Now we can directly see, why the branch of primary cutting open points in γ is not continued beyond s_k: A trajectory starting there *exits* $\bar{T}$ close to b_k and hence is not a regularly touching trajectory.

(b) A trajectory representing the second kind touches S slightly above b_k and exits $\bar{T}$ close to c_k. This is a typical type II behavior and shows why the secondary branches of φ end at the points c_k.

(c) The last kind of trajectory also touches S in (x_c, x_w), but does so a little below b_k this time, then comes close to c_k, but remains inside of $\bar{T}$, and eventualy exits this region close to the first branch of φ. This second type II situation makes it clear why the secondary branches of φ start out in a point of its first branch, and it moreover gives the reason why a τ-interval has to be cut out from the domain of φ: The latter trajectory stays for more than one half turn (π/ω) around the real eigenvector longer inside of $\bar{T}$ than the trajectory described in (b) does.

Thus, it becomes obvious why type III *separates separating structures*. Since no trajectory can touch S more than twice, no further principal type of behavior exists. Additional complexity arises from the number of doubly touching trajectories being involved. The sequence of these special orbits, as we saw, exhibits a universal property of the saddle-focus dynamics. It results from the fact that subsequently "born" doubly touching trajectories differ essentially only by an extra turn around the real eigenvector of the steady state, a result that holds true exactly both for $\varrho/\omega \to 0$ $(k \to \infty)$ and for $\varrho/\omega \to \infty$.

To conclude, the formalism of Poincaré halfmaps allows one to state precisely the *conditions on the parameters* for the appearance of the different separating mechanisms (cf. [2]). Moreover it also yields the *boundaries of the regions in state space* where these mechanisms are effective. All results, as soon as achieved, can be used directly to interpret prototypic dynamical evolutions of the present dynamical system.

Acknowledgement

I thank O. E. Rössler for discussions and for pointing out the importance of the work of Arneodo, Coullet, and Tresser. This paper was supported in part by the DFG.

[1] C. Kahlert and O. E. Rössler, Z. Naturforsch. **40 a,** 1011 (1985).
[2] C. Kahlert and O. E. Rössler, The Separating Mechanisms in Poincaré Halfmaps, Z. Naturforsch. **41 a** (1986), in press.
[3] C. Kahlert and O. E. Rössler, Z. Naturforsch. **38 a,** 648 (1983).
[4] L. P. Shil'nikov, Sov. Math. Docl. **6,** 163 (1965).
[5] A. Arneodo, P. H. Coullet, and C. Tresser, Commun. Math. Phys. **79,** 573 (1981).
[6] C. Kahlert and O. E. Rössler, Z. Naturforsch. **39 a,** 1200 (1984).
[7] C. Kahlert, Z. Naturforsch. **41 a,** 567 (1986).
[8] C. Kahlert, Infinite Nonperiodic Wavetrains in a Class of Reaction-Diffusion-Equations – Analytical Properties of Poincaré Halfmaps (in German), Ph.D. Thesis, University of Tübingen, 1984.
[9] C. Kahlert and L. O. Chua, Transfer Maps and Return Maps for Piecewise-Linear Three-Region Dynamical Systems, Int. J. Circuit Theory and Applications **14** (1986), in press.
[10] B. Uehleke and O. E. Rössler, Z. Naturforsch. **39 a,** 342 (1984).
[11] C. Kahlert, The Composition of Poincaré Halfmaps and Chaotic Attractors, in preparation.